

pubs.acs.org/Macromolecules Article

Understanding How Metal—Ligand Coordination Enables Solvent Free Ionic Conductivity in PDMS

Xinyue Zhang, Jinyue Dai, Max Tepermeister, Yue Deng, Jingjie Yeo, and Meredith N. Silberstein*



ACCESS I



Metrics & More

Article Recommendations

Supporting Information

P-PV/LiOTH

P-PV/LiOTH

P-PV/Cu(OTf)₂1

P-PV/Cu(OTf)₂1

P-PV/Cu(OTf)₂1

Sample species

ABSTRACT: Ionically conductive polymers are commonly made of monomers containing high polarity moieties to promote high ion dissociation, like poly(ethylene oxide) (PEO), polyvinylidene difluoride (PVDF), and poly(vinyl alcohol) (PVA). However, the glass transition temperatures ($T_{\rm g}$) of these polymers are relatively high, and therefore, these polymers are in a glassy state at room temperature, which limits the mechanical flexibility of the material. Although polydimethylsiloxane (PDMS) has many attractive physical and chemical properties, including a low glass transition temperature, mechanical flexibility, and good biocompatibility, its low dielectric constant suppresses ion dissociation. In this Letter, we overcome this shortcoming by functionalizing the PDMS with ligands that can form labile coordination with metal ions, which greatly promotes ion dissociation and improves the ionic conductivity by orders of magnitude. By combining an experimental study with a fully atomistic molecular dynamics simulation, we systematically investigated the ion transport mechanisms in this low $T_{\rm g}$ material.

■ INTRODUCTION

Ionically conductive polymers, also commonly referred to as polymer electrolytes, are emerging as popular material candidates for enabling cutting-edge technologies, including energy storage, soft robotics, biomedical devices, and bioinspired sensory systems. 1-5 In recent decades, liquid-, gel-, and solid-state ionically conductive polymers have been developed to fulfill various needs. For example, most of the pioneering studies on polymer electrolytes are based on poly(ethylene oxide) (PEO) complexed with alkali metal salts.^{6,7} Ionic liquids have been either mixed into neutral polymer networks or polymerized into poly(ionic liquid)s (PILs) for engineering various electrochemical devices.^{8,9} Ionic polymer metal composites (IPMC) consisting of a polyelectrolyte membrane placed between two noble metal electrodes have been studied to enable large actuation under an applied electric field. 10 Continued effort has been made to both develop novel ionically conductive polymers and understand fundamental ion conducting mechanisms to enable rational design based on functional requirements for a particular application.

Ion mobility and ion concentration are the two key factors governing ionic conductivity of a polymer; the former is not only directly related to the identity and quantity of cations and anions but is also greatly affected by the physical and chemical characteristics of the polymer matrix bearing the ions. 11 Polymers with a low glass transition temperature and low crystallinity are good candidates to achieve high ionic conductivity at room temperature for practical applications. 12 However, polyelectrolytes predominantly have high polarity backbones to facilitate ion dissociation, which raises the glass transition temperature or promotes crystallinity by increasing intermolecular interactions.¹³ In contrast, polymers with low dielectric constants, like PDMS, have low glass transition temperatures and maintain an amorphous state but are barely ionically conductive due to poor salt dissociation.¹⁴ Metalligand coordination as a noncovalent interaction has been extensively applied in polymer matrices to enhance the mechanical toughness, tune viscoelasticity, and enable selfhealing. 15-20 In recent years, metal-ligand coordination has

Received: December 15, 2022 Revised: March 22, 2023 Published: April 13, 2023





also been studied as a means of designing ionically conductive polymers. $^{21-24}$ For example, imidazole-and imidazolium-containing polymers, which can bind to metals, have been synthesized and studied. 25,26 This moiety is particularly interesting due to its wide prevalence in nature and in the human body and is therefore relevant in bioactive applications. In addition, polymer electrolytes containing metal—ligand coordination such as Li $^{+}$ coordinated poly(N-methyl-malonic amide) and Zn $^{2+}$ coordinated polyacrylamide have been developed for all-solid-state batteries. 27,28

It is vital to build a fundamental understanding of the ion conducting mechanisms of these amorphous, elastomeric, metal-coordinated polymers and the relation of these mechanisms to the polymer structure. Molecular dynamics (MD) simulations are a powerful approach to provide detailed insight into transport phenomenon in ionic polymeric materials at the atomistic level.^{29,30} So far, MD simulations related to ionic conductivity have mainly focused on collecting single ion dynamics. Ionic conductivity is commonly determined with the Nernst-Einstein (NE) equation, which gives conductivity as directly proportional to the diffusion coefficients of the ions. The NE approximation works well for dilute systems with high dielectric constants, but fails in the concentrated ion regime.³¹ An alternative approach by Wheeler and Newman following a Green-Kubo methodology in the Stephan-Maxwell framework reported a large noise for determining off-diagonal transport coefficients.³³ Grossman et al. proposed the cluster Nernst-Einstein (cNE) method that accounts for salt nucleation.³⁴ They showed that their method could reproduce the experimental results of PEO-based electrolytes at a high salt loading.³⁴ Their method should be applicable to other cases with solvent-free or low dielectric constant, where the capacity to dissociate ion pairs is relatively weak, and therefore the ions form clusters.

In this study, we combine in-depth experimental studies with fully atomistic MD simulations to unveil ion conducting mechanisms in metal-coordinated PDMS. A low molecular weight polydimethylsiloxane (PDMS) end-functionalized with pyridyl imine ligands is selected as the model system, and a series of Li and Cu salts is added to form polymer complexes. Factors that govern the ionic conductivity of the material, including ion dissociation, ion concentration, and chain mobility, are discussed in the context of the metal-ligand coordination density and strength. First, we highlight that the formation of metal-ligand coordination promotes salt dissociation into ions and therefore enhances the ionic conductivity of the PDMS complex as compared to the direct mixing of pristine PDMS and metal salt. Next, we show that the choice of metal cation, counteranion, and ion concentration can vary the ionic conductivity of PDMS by orders of magnitude due to the distinct cation-anion interactions. To elucidate the ion transport mechanisms, a range of properties are computed from the MD simulations, including ion and polymer chain diffusion coefficients, ionic conductivity, and salt clustering. Furthermore, based on our observations of the single metal cation coordinated PDMS, we propose and prove that a synergistic effect on the mechanical strength and ionic conductivity of the PDMS can be achieved by coordinating with two metal cation species: the majority component is the metal cation with weak coordination, which is primarily responsible for the ion conductivity, whereas the minority component is the metal cation with strong coordination that enhances the mechanical strength of the network. This paper

provides insights into the strategic design of ionically conducting polymers that would benefit a range of applications.

■ RESULTS AND DISCUSSION

Effect of Metal-Ligand Coordination. To understand how metal-ligand coordination promotes the ionic conductivity of a polymer, we chose low molecular weight PDMS as the polymer precursor because of its many advantageous features. First, PDMS has a low glass transition temperature ($T_g \approx -123$ °C), yielding dynamic chain motion at room temperature, which facilitates the transport of ions. Second, PDMS has low inherent ion impurity content³⁷ and low dielectric constant ($\kappa \approx$ 2.3-2.8),38 which serves as a nonconductive baseline and creates a clear contrast in the ionic conductivity of the polymer before and after introducing metal-ligand coordination. Furthermore, ion interaction in the system is mainly mediated by the metal-ligand coordination rather than the solvation of the polymer backbone, which offers us a good model to decouple the effect of metal-ligand coordination from other factors that contribute to the ionic conductivity. 14,39 Third, PDMS has many good physical and chemical properties, such as being stretchable and inert. Finally, PDMS is easy to fabricate and low cost, which makes it a popular material candidate for next-generation ionic devices. 5,40

We created a model system by functionalizing the ends of low molecular weight PDMS with a metal coordinating ligand. Pyridyl imine is selected as the functional group because it is a versatile ligand that can coordinate with various metal cations.⁴ The model system (P-PI, P represents PDMS, PI represents pyridyl imine ligand) is synthesized via a condensation reaction between aminopropyl terminated PDMS (P-NH₂, NH₂ represents amine end group) and 2-pyridinecarboxaldehyde according to a previously reported procedure, yielding a yellow oil-like product (Figure 3a). 42 The structure of P-PI is confirmed by ¹H NMR (Figure S1). Based on the ratio of the hydrogen atoms in the dimethylsiloxane backbone to the hydrogen atoms in the pyridyl imine end groups, which is calculated from the integration of different peak areas in the ¹H NMR spectrum, the number-average molecular weight (M_n) of P-PI is around 2000 g/mol. The dielectric constant for P-NH₂ of this molecular weight is measured to be 3.3, with a slight decrease to 3.1 for P-PI.

To study how the formation of coordination complexes affects the ionic conductivity of the model system, a monovalent metal cation, Li⁺ is added. Since Li⁺ has a coordination number of 4-6 with different ligand molecules, it is important to determine the coordination stoichiometry between Li+ and the pyridiyl imine ligand. 43,44 Therefore, a small-molecule model ligand, Npropyl(2-pyridyl)methanimine, is synthesized (Figure S2), and it is combined with lithium trifluoromethanesulfonate (LiOTf) salt to form a small-molecule Li⁺-pyridyl imine complex. This complex is analyzed by mass spectrometry (MS) in electrospray ionization (ESI) positive ion mode, and the molecular ion peak is found to be 453.18 m/z, indicating that the ratio between Li⁺ and the pyridyl imine ligand is 1:2 (Figure S3). Since pyridyl imine groups are present at both ends of the PDMS chain, this number implies that the ligands are fully coordinated with Li⁺ when the molar ratio of PDMS to LiOTf is 1:1.

Next, a polymer complex with this 1:1 molar ratio of pyridyl imine functionalized PDMS to LiOTf is synthesized (P-PI/LiOTf1, Figure 1a). Two additional polymers are used as controls: (1) P-PI with no LiOTf salt and (2) pristine PDMS mixed with same quantity of LiOTf salt ($P-NH_2/LiOTf1$,

(a)
$$\begin{array}{c}
(a) \\
(b) \\
(b) \\
(c) \\
(c) \\
(d) \\
(d) \\
(e) \\$$

Figure 1. Comparison between the model and the control systems. The chemical structure and schematic of (a) the LiOTf coordinated PDMS, P-PI/LiOTf1; (b) the mixture of pristine PDMS and LiOTf, P-NH₂/LiOTf1. Schematics show the expected different degrees of cation—anion dissociation in the PDMS with and without ligand functionalization.

Figure 1b). It is worth highlighting that additional solvent is not necessary to facilitate the mixing of the PDMS and LiOTf salt in the preparation of P-PI/LiOTf1 and P-NH2/LiOTf1, because LiOTf salt can slowly but completely dissolve in the PDMS under vigorous stirring. This is in contrast to the conventional preparation procedure, which uses solvent casting followed by solvent evaporation to prepare dry polymer electrolytes. 45 Given that organic solvents are hard to completely remove even after careful vacuum drying, causing variation in the measurement of ionic conductivity, we think it is advantageous that this model system does not require extra solvents to synthesize Li⁺ coordinated samples. ¹¹ The formation of a complex between the PDMS and Li⁺ is verified by Fouriertransform infrared spectroscopy (FTIR) (Figure S5). The IR spectra of the samples are normalized by the intensity of the peak at 1259 cm⁻¹, corresponding to CH₃ symmetric bending in Si-CH₃ on the PDMS backbone. 46 Compared to the spectrum of P-PI, in P-PI/LiOTf1 the absorbance intensity at a wavenumber of 1650 cm⁻¹ decreases, and a new peak rises at a lower wavenumber of 1593 cm⁻¹. This peak shift results from

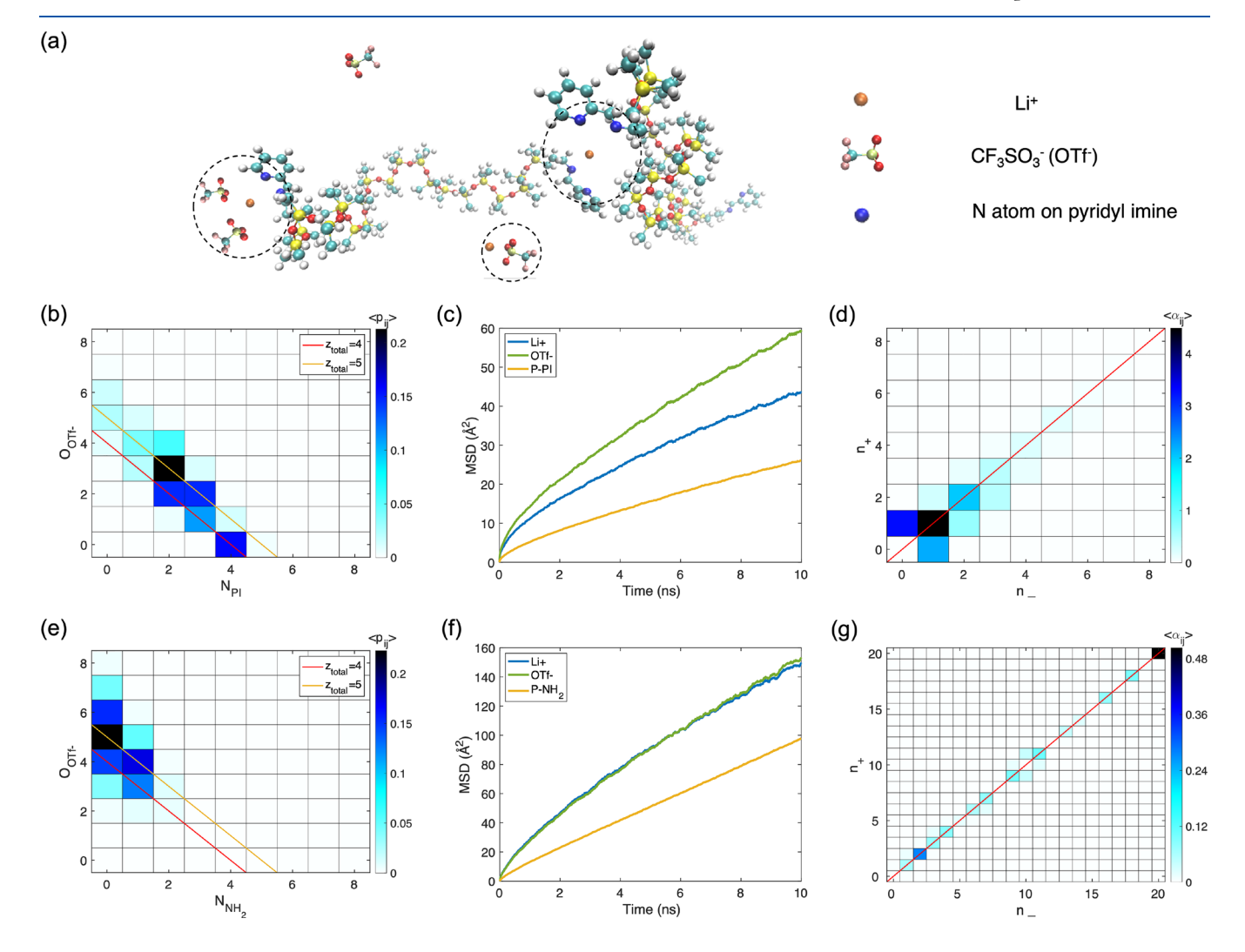


Figure 2. MD simulation setup and results. (a) Schematic representation of different Li⁺ coordination environments within P-PI/LiOTf1. (b-d) Results of P-PI/LiOTf1 and (e-g) results of $P-NH_2/LiOTf1$. (b, e) Coordination matrix that presents the relative contribution to the total coordination of Li⁺ by oxygens from OTf⁻ and nitrogens from the end groups of the polymer chains. The grid squares passed through by the red and yellow line represent the most favorable total coordination numbers of 4 and 5. p_{ij} is the probability of each coordination combination over the simulation time. (c, f) MSD plot of cations, anions, and polymer chains. (d, g) Ion clustering statistics, where the grid squares passed through by the red line represent the neutral clusters. $α_{ij}$ is the average count of each cluster over the simulation period.

the decreased bond order of C=N stretching in the coordinated pyridyl imine ligands.⁴⁷ The presence of OTf^- anions is confirmed by the new peaks between wavenumbers of 1230 cm⁻¹ and 1300 cm⁻¹ from the overlapped C-F and S=O stretching.⁴⁸

We then compare the ionic conductivity of the model and controls using electrochemical impedance spectroscopy (EIS), which shows distinct results in Nyquist plots (Figure S6). P-PI has an extremely low ionic conductivity that is below the limit of detection because of the low ion impurity content (σ < 4.8 × 10^{-10} S/m). In contrast, the ionic conductivity of **P-PI/LiOTf1** increases by at least 5 orders of magnitude, yielding the value of $(4.28 \pm 0.22) \times 10^{-5}$ S/m. Although P-NH₂/LiOTf1 also shows improved ionic conductivity ($\sigma = (2.51 \pm 0.12) \times 10^{-6} \text{ S/}$ m) compared to the pure PDMS, it is only about 6% of the value of P-PI/LiOTf1. Since the same amount of LiOTf salt is added to the PDMS with and without ligand functionalization, we infer that the extent of salt ionization determines the ionic conductivity of the material.³⁹ The significantly higher ionic conductivity of P-PI/LiOTf1 compared to that of P-NH₂/ LiOTf1 demonstrates that the formation of metal-ligand coordination facilitates cation-anion dissociation and therefore improves the ionic conductivity of the PDMS.

To provide critical molecular level insights that are hard to capture by experimental characterization techniques, fully atomistic molecular dynamics (MD) simulations are performed with the Large Atomic Molecular Massive Parallel Simulator (LAMMPS) (Figure 2a).⁴⁹ The molecular interaction is described by using the polymer-consistent force field (PCFF).⁵⁰ Each simulated system consists of 20 PDMS chains, each 21 monomers long, and 20 LiOTf molecules, equivalent to the experimentally characterized structure. A full description of the MD simulation methods is provided in the experimental section and Supporting Information (section 3). Results for MD simulated P-PI/LiOTf1 and P-NH₂/LiOTf1 are given in Figure 2b-d and Figure 2e-g, respectively.

With the equilibrated MD system, we first compared the polymer-salt interactions in P-PI/LiOTf1 and P-NH₂/ LiOTf1. From the coordination matrices shown in Figure 2b and Figure 2e, Li⁺ tends to interact with different electronegative moieties in the two system. In P-PI/LiOTf1, Li⁺ has a strong tendency to coordinate both the nitrogen atom on the pyridyl imine group and the oxygen atoms on OTf. In P-NH₂/ LiOTf1, Li⁺ preferably interacts with the oxygen atoms on OTf-. It is worth noting that the most favorable lithium coordination is 4 and 5, consistent with previous work by Olsher et al.⁵¹ The geometries of most 4-fold coordination and 5-fold coordination structures are found to be close to tetrahedral and square-pyramidal by visualization with Visual Molecular Dynamics (VMD)⁵² software. In addition, the coordination matrix in Figure S12 indicates that Li⁺ barely interacts with the siloxane group on the PDMS backbone. The coordination analysis based on simulation is consistent with our mass spectroscopy experimental results, confirming that the most probable structure is 4-fold coordination, which helps to validate the transferability of the PCFF force field to the PDMS and salt system.

To better understand the effect of metal—ligand coordination on ion and chain mobility, we investigated the diffusion coefficient of different components in the MD simulations of these two material systems. The MSD plots of ions and polymer chains for **P–PI/LiOTf1** are shown in Figure 2c. Both Li⁺ and OTf⁻ motion is subdiffusive before 5 ns, i.e., MSD $\propto \tau^{\alpha}$ with α <

1. At times longer than 5 ns, the ion motion becomes diffusive, and the diffusion coefficient can be obtained from the MSD by applying the Einstein relation (Equation 1). The OTf diffusion coefficient ($D_{OTf} = 1.12 \text{ Å}^2/\text{ns}$) is larger than the Li⁺ diffusion coefficient ($D_{Li}^+ = 0.84 \text{ Å}^2/\text{ns}$). These results show that both cations and anions are mobile in the polymer matrix with anions having higher mobility than cations. We infer that the motion of cations is mainly through the ligand exchange process and is slowed down by this transient coordination interaction; in contrast, anions are less confined, and the motion is facilitated by chain segmental motion. The PDMS (P-PI) chains also diffuse over time, but at a substantially slower rate than the ions. For P-NH₂/LiOTf1, the MSD curves of cations and anions (Figure 2f) almost coincide with similar diffusion coefficients of $D_{Li}^+ = 2.75$ $Å^2/\text{ns}$ and $D_{\text{OTf}} = 2.78 \, Å^2/\text{ns}$). This is due to the poor solvation ability of pristine PDMS, which promotes the formation of ionic clusters and results in the cations and anions diffusing together. Interestingly, the diffusion coefficients of both the ions and the chains in P-NH₂/LiOTf1 are about three times larger than their values in P-PI/LiOTf1, resulting from the fact that ion motion in P-NH₂/LiOTf1 encounters less confinement from the PDMS chains due to minimal coordination. At first glance, this seems contrary to our experimental results, since ionic conductivity is typically thought to be directly related to the diffusion coefficient. However, the presence of ionic clusters instead of single ions significantly decreases the quantity of charge carriers in the system and therefore yields a low ionic conductivity of the material.

Ion clustering is a common phenomenon at high salt concentrations or when the interaction with the local structure is not strong enough for salt ionization, leading to correlated motion of cations and anions.⁵³ According to the cluster Nernst-Einstein (cNE) approach developed by Grossman et al., the net charge and diffusivity of each ionic cluster are aggregated to give the overall system conductivity (i.e., neutral clusters do not contribute to conductivity, Equation 3).³⁴ The cluster populations of P-PI/LiOTf1 and P-NH₂/LiOTf1 are shown in Figures 2d and 2g, respectively. For P-PI/LiOTf1, both charged clusters and neutral clusters are observed at thermodynamic equilibrium, with clusters composed of up to 12 ions (6 cations and 6 anions). For P-NH₂/LiOTf1, the cluster analysis shows an increase of cluster size, up to all of the ions in the simulation box (into a single cluster). The formation of very bulky neutral ionic clusters explains the lower ionic conductivity compared with that of P-PI/LiOTf1 measured from experiments. More importantly, it demonstrates that by introducing ligands onto the polymer chains, the formation of metal-ligand coordination reduces large neutral ionic aggregation and facilitates the transport of charge carriers, improving the conductivity. Using the cNE eq (Equation 3), we find conductivity for P-PI/LiOTf1 is 0.0041 S/m, while that for P-NH₂/LiOTf1 is 0.00036 S/m. The ratio of the ionic conductivity with ligands to that without is about 11.4 times, which matches well with the ratio of 17 from the experiments. Without the cluster correction on the NE equation, the ionic conductivity would be 0.036 S/m and 0.11 S/m for P-PI/ LiOTf1 and P-NH₂/LiOTf1, which would contradict the experimental results. We note here that while our trends match well with experiments, our predicted conductivity values are substantially above the experimentally measured values. We believe this has to do with the scaled representation of the cation-anion interaction strength, which will be discussed in more depth when we compare the results for different anions.

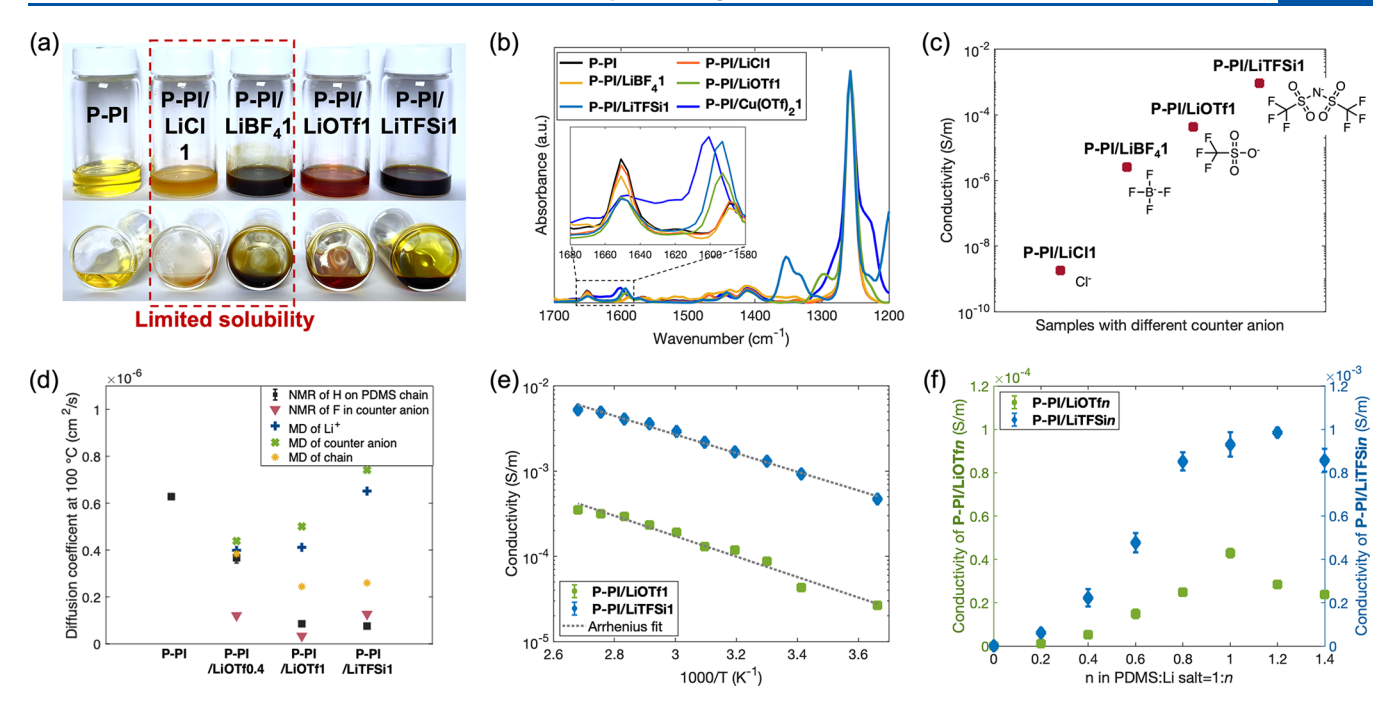


Figure 3. Li⁺ coordinated PDMS. (a) Both front view and bottom view photos of the ligand-functionalized PDMS and the Li⁺ coordinated PDMS containing different counteranions. P-PI/LiCl1 and P-PI/LiBF₄1 have undissolved salt at the bottom of the vials, whereas P-PI/LiOTf1 and P-PI/LiTFSi1 yield a clear product. (b) IR spectra of the PDMS precursor and the metal coordinated PDMS. (c) Ionic conductivity of the Li⁺ coordinated PDMS with varying counteranions. (d) A comparison of diffusion coefficients from both experimental and simulation results: diffusion coefficients of ¹H from PDMS chain and ¹⁹F from counteranions in Li salts are obtained from PFG SE NMR measurements at 100 °C, and diffusion coefficients of Li⁺ and counteranions are obtained from MD simulation at 100 °C. Error bars are calculated from ¹H in different moieties on the PDMS chain. (e) Ionic conductivity as a function of temperature for P-PI/LiOTf1 and P-PI/LiTFSi1. (f) Ionic conductivity of LiOTf and LiTFSi coordinated PDMS with varying salt concentrations.

Next, we are interested in assessing whether interchain cation hopping via continuous ligand exchange is an important transport mechanism for cations. We suspect cation hopping might be important, because the MSD plots show that chain motion is 2-3 times slower than Li⁺ diffusion, indicating that cation diffusion, on this time scale, is not solely driven by the segmental motion of the polymer. The hopping behavior varies considerably among the individual cations. In Figure S8 and Figure S9 we show the behavior of two example ions: the less diffusive Li⁺ tends to attach to one ligand from one chain over the entire 80 ns simulated while exchanging among other ligands from different chains; the more diffusive Li⁺ hops frequently between chains. It is shown in Figure S10 that Li+ jumping among polymer chains is more frequent in P-NH₂/LiOTf1 than in P-PI/LiOTf1, due to the weak polymer-ion interaction and hence short residence time when there is no ligand. In addition, the motion of Li⁺ along the host chain is insignificant for this material system, contrary to other polymer-salt systems like PEO electrolytes, 54 because only the ligand grafted on the ends of the chains can coordinate with the lithium ions, while the monomers hardly interact with Li⁺ due to the nonpolar nature of PDMS. The radial distribution function (RDF) plot of oxygens within the PDMS backbone relative to the lithium ions supports this lack of association, showing an average coordination number of zero (Figure S13).

Effect of Counteranions. Since varying the counteranion in a metal—ligand complex can yield distinct coordination strength and lifetime, a series of Li⁺ coordinated PDMS with different anion species is synthesized to study the influence of counterions on ionic conductivity. Another three Li salts, lithium chloride (LiCl), lithium tetrafluoroborate (LiBF₄), and

lithium bis(trifluoromethanesulfonyl)imide (LiTFSi) are added into the ligand functionalized PDMS at the same 1:1 molar ratio (P-PI/LiCl1, P-PI/LiBF₄1, and P-PI/LiTFSi1, respectively), which show distinct solubilities after rigorous mixing. P-PI/LiCl1 had a large amount of undissolved salt at the bottom of the container. P-PI/LiBF₄1 also had an observable amount of undissolved salt left after thorough mixing. P-PI/ LiTFSi1 is fully dissolved in the PDMS oil and yields a more viscous liquid with a darker color than P-PI/LiOTf1 (Figure 3a). The differences among the Li⁺ coordinated PDMS containing different counteranions can also be seen from their IR spectra (Figure 3b). Comparing to the spectrum of P-PI, the C=N stretching peak at the wavenumber of 1650 cm⁻¹ is partially shifted to 1593 cm⁻¹ due to the formation of Li⁺-pyridyl imine coordination in the spectrum of P-PI/LiTFSi1.⁵⁶ The peaks at the wavenumber of 1300-1380 cm⁻¹ are from the overlapped C-F and S=O bond stretching in TFSi⁻ anions. ⁵⁷ Conversely, the spectra of P-PI/LiCl1 and P-PI/LiBF₄1 are quite similar to P-PI; the peak shifts caused by coordination and the presence of counteranions are barely detectable.

The ionic conductivity of the Li $^+$ coordinated PDMS with different counteranions is measured by EIS and shows orders of magnitude differences: P-PI/LiCl1 < P-PI/LiBF $_4$ 1 < P-PI/LiOTf1 < P-PI/LiTFSi1 (Figure 3c, Figure S14, Table S4). The ionic conductivity of the Li $^+$ coordinated PDMS increases with the size of the counteranion. Bulkier counteranions such as OTf $^-$ and TFSi $^-$ have higher charge delocalization, yielding weaker cation—anion interaction, and therefore the increased ion mobility promotes higher ionic conductivity. In contrast, the smaller anions such as Cl $^-$ and BF $_4$ $^-$ have stronger electrostatic attraction with Li $^+$, which results in a more

significant cation—anion association. ⁵⁸ This explains the limited salt solubility in PDMS, and moreover, the low ion concentration and low ion mobility together lead to low ionic conductivity. The MD simulations of **P**–**PI/LiTFSi1** also show greater ionic conductivity than **P**–**PI/LiOTf1** (σ_{TFSi}^- = 0.0054 S/m vs σ_{OTf}^- = 0.0041 S/m), though the trend is less prominent than the experimental one. At 30 °C, the ionic conductivity from MD simulations for **P**–**PI/LiTFSi1** is about 3 times higher than the experimental value, and it is about 46 times higher than the experimental value for **P**–**PI/LiOTf1**. The reason for the large discrepancy in **P**–**PI/LiOTf1** could be the underestimation of ionic correlation strength due to the use of a scaling charge factor, leading to greater diffusivity as molecular sizes decrease.

To gain a more quantitative insight into the mobility of the PDMS chain and counteranions, Pulsed-field-gradient (PFG) spin—echo (SE) NMR is performed to investigate the self-diffusion of the system. ^{23,59} The dynamics of the PDMS chains are quantified on the basis of the stimulated-echo signal attenuation of ¹H spectra (note: the self-diffusion coefficient of ¹H is not quantitatively identical to the self-diffusion coefficient of the PDMS chain, but they are strongly correlated), and the self-diffusion coefficient of counteranions is calculated from the stimulated-echo signal attenuation of ¹⁹F (Figure 3d, Figure S15, Figure S16, and Table S5). 23,60 It is worth noting that since the PDMS samples are not diluted by any solvent, the experimentally measured self-diffusion coefficients directly reflect the actual dynamics of the material. Comparing the diffusion coefficients in P-PI/LiOTf1 and P-PI/LiTFSi1, we can see that the mobility of the hydrogens on the PDMS chains is similar in P-PI/LiTFSi1 and P-PI/LiOTf1, whereas the mobilities of counteranions are quite different: TFSi⁻ is higher than that of OTf-. MD simulations of P-PI/LiTFSi1 compared to P-PI/LiOTf1 show that the bulkier, less polar TFSi anion tends to have more frequent intercluster hopping, leading to an overall higher diffusivity ($D_{\text{TES}_{i}}^{-} = 1.66 \text{ Å}^2/\text{ns}, D_{\text{L}_{i}}^{+} = 1.26 \text{ Å}^2/$ ns). This difference is also confirmed by Very Low Frequency EIS (VLFEIS) transference number experimental measurements. 61 P-PI/LiTFSi1 has a much smaller transference number than P-PI/LiOTf1 (0.07 vs 0.24) which confirms that more of the current is carried by counterions and negatively charged clusters in P-PI/LiTFSi1 than in P-PI/LiOTf1. The cluster analysis from MD observations is provided in Figure S18, which is consistent with previous work on PEO-LiTFSi systems: there are mostly neutral ion pairs but also a non-negligible concentration of negatively charged clusters, resulting in an overall asymmetric distribution.⁶² The distribution of charged clusters in P-PI/LiTFSi1 is less symmetric compared to that of P-PI/LiOTf1, with overall more negatively charged clusters present in the system, indicating that Li⁺ from P-PI/LiTFSi1 interacts more strongly with the polymer chains than does Li⁺ from P-PI/LiOTf1. Furthermore, the diffusion coefficients of positively charged clusters tend to be slightly smaller than those of negatively charged clusters with the same constituent number of ions, due to the stronger local interaction between positively charged clusters and electronegative ligands on the polymer. The transference numbers calculated from MD simulations are 0.253 for P-PI/LiOTf1 and -0.313 for P-PI/LiTFSi1. The negative transference number for P-PI/LiTFSi1 confirms the existence of negatively charged clusters dominating Li+ transport. Further discussion of the MD calculated transference number is provided in SI Section 4.6.

The ionic conductivity of P-PI/LiOTf1 and P-PI/LiTFSi1 as a function of the ambient temperature T from 0 to 100°

(Figure 3e and Figure S17) is measured experimentally. The logarithmic scale of ionic conductivity is found to be linearly proportional to 1000/T, following Arrhenius behavior $\sigma \sim \exp(-E_a/RT)$, where E_a is an apparent activation energy, R is the universal gas constant, and T is the absolute temperature. S9,63 The apparent activation energy is the slope of the fit line, which is quite similar in P-PI/LiOTf1 and P-PI/LiTFS11 (22.98 and 20.96 kJ·mol⁻¹ respectively). We believe that the apparent activation energy is the combination of the energy barriers of (1) the cation—anion interaction of the Li salt and ion clusters; (2) dissociation of Li⁺ from the connected ligands; and (3) the self-diffusion of the PDMS chain that facilitates ion motion. 11,36,59

Effect of Ion Concentration. We study the effect of ion concentration on the ionic conductivity of the model system by preparing a series of LiOTf and LiTFSi coordinated PDMS with different salt concentrations (P-PI/LiOTf0.2 to P-PI/ LiOTf1.4 and P-PI/LiTFSi0.2 to P-PI/LiTFSi1.4, the number in the sample name indicates the molar ratio of PDMS:LiOTf = 1:n). In both cases, the ionic conductivity of the PDMS complex first increases and then decreases as the Li salt concentration increases; the highest ionic conductivity is reached around the maximum coordination capacity of the ligands with Li⁺ cations (corresponding to PDMS:Li salt = 1:1, Figure 3f, and Table S8). This indicates that at first, more Li⁺ cations and counteranions exist in the system as the Li salt concentration is increased, improving the ionic conductivity. However, when the ligand coordination capacity is oversaturated by excess Li salt, the ionic conductivity of the PDMS complex starts to decrease monotonically (Figure S22). As seen from both the previous studies and our MD simulation (Figure S23), ion pairs and higher-order clusters form at high Li salt concentration, which hinders the effective cation-anion dissociation and ion transport, thereby decreasing the overall ionic conductivity. 32,63,64

We can look more deeply into the mechanism of the salt concentration dependence with PFG SE NMR and MD simulations. It can be clearly seen from the trend of P-PI, P-PI/LiOTf0.4, and P-PI/LiOTf1, that the segmental motion of the PDMS chains slow down when forming complexes with LiOTf, and decrease further at a higher LiOTf concentration (Figure 3d), because the formation of metal-ligand coordination adds temporary constraints to the chain ends. 19 The diffusion of OTf also slows at higher LiOTf concentration, confirming that the anion motion is associated with the chain motion. Interestingly, while the MD calculated diffusion at 100 °C also shows decreased chain mobility at increased LiOTf concentration, it actually shows a slight increase in ion diffusivity. The MD result would suggest that the thermally enhanced clustering 65,66 is more important than the reduced chain mobility at increased concentration, in contrast to the experimental result.

Effect of Cation Identity. We next study the effect of coordination strength on the ionic conductivity of the metalligand coordinated PDMS by using a multivalent cation, Cu^{2+} . To obtain the coordination structure, a small-molecule Cu^{2+} pyrdiyl imine complex is synthesized by adding copper trifluoromethanesulfonate ($Cu(OTf)_2$) into the model ligand N-propyl(2-pyridyl)methanimine. The molecular ion peak of the complex is analyzed by MS in ESI positive ion mode and found to be 689.05 m/z, confirming the ratio between Cu^{2+} and pyridyl imine ligand is 1:2 (Figure S4). 20,67 A series of $Cu(OTf)_2$ coordinated PDMS with different salt concentrations is synthesized ($P-PI/Cu(OTf)_20.2$ to $P-PI/Cu(OTf)_21$, the

number in the sample name indicates the molar ratio of PDMS: $Cu(OTf)_2 = 1:n$). We expect that Cu^{2+} forms a stronger and more stable complex than Li+, yielding a less dynamic network, which can be characterized by the rheology of the PDMS complexes. The linear viscoelastic (LVE) region of each material is first determined by running a strain sweep at a frequency of 1 Hz (Figure S24), ⁶⁸ which shows that the critical strain of P-PI/Cu(OTf)₂1 is near 1%. An oscillation strain of 0.1% is therefore chosen to perform the frequency sweep for all of the samples (Figure 4a). We first compare the coordination strength of Li⁺ and Cu²⁺ by examining the rheological curves of P-PI/LiOTf1 and P-PI/Cu(OTf)21: the storage and loss moduli (G' and G'', respectively) of $P-PI/Cu(OTf)_21$ are orders of magnitude higher than the moduli of P-PI/LiOTf1 within the full frequency range measured. In $P-PI/Cu(OTf)_2I$, G' > G'' and G' remains independent of the frequency, indicating that the material is in the rubbery plateau region due to the presence of strong metal-ligand coordination, which act as transient cross-links in the polymer; whereas in P-PI/ **LiOTf1**, G' < G'', indicating that the material is in the terminal region, where chains relax quickly and the material behaves like a viscoelastic fluid.⁶⁹ The difference in viscoelasticity of the Li⁺ and Cu²⁺ coordinated PDMS can also be directly seen from the photos of P-PI/LiOTf1 and P-PI/Cu(OTf)₂1 samples: the former is a viscous liquid, and the latter is a flexible film, confirming that Cu2+ yields much stronger bonding with the ligand functionalized PDMS than Li^+ . The variation of polymer viscoelasticity of the Cu²⁺-coordinated PDMS as a function of Cu(OTf)₂ concentration is also shown in the rheology plot: the material transforms from a viscoelastic fluid to a viscoelastic solid with an increasing Cu(OTf)₂ concentration. A crossover between the storage and loss modulus arises and shifts to the lower frequency at higher Cu(OTf)₂ concentration, indicating that the characteristic relaxation time of the PDMS is significantly prolonged when it is cross-linked by Cu(OTf)₂. ¹⁹ The change in polymer dynamics caused by using the more strongly coordinated Cu²⁺ or increasing the Cu salt concentration also results in the increase in $T_{\rm g}$, which is measured by differential scanning calorimetry (DSC) (Figure 4b). The $T_{\rm g}$ of P-PI/LiOTf1, P-PI/Cu(OTf)₂0.2, P-PI/Cu(OTf)₂0.4, and $P-NH_2/Cu(OTf)_21$ is below the testing limit of the machine $(-90 \, ^{\circ}\text{C})$, so no slope change is seen on the heat flow curve. However, the T_g values of $P-PI/Cu(OTf)_20.6$, $P-PI/Cu-(OTf)_20.8$, and $P-PI/Cu(OTf)_21$ increase to around -38 °C, -30 °C, and -28 °C, respectively. The dramatic increase in $T_{\rm g}$ reflects the reduction of chain mobility, which should confine ion transport. 59,70

To study how the coupled Cu2+ ion concentration and network dynamics together affect the ionic conductivity of the material, we measure the ionic conductivity of the PDMS complex as a function of Cu(OTf)₂ concentration, showing quite a different from that in the Li⁺ coordinated system (Figure 4c). We note that the Cu(OTf)₂ coordinated PDMS, regardless of salt concentration, cannot achieve nearly as high a conductivity as the maximum value of the LiOTf coordinated PDMS. The maximum ionic conductivity is obtained at P-PI/ Cu(OTf)₂0.4, which is far lower than the maximum coordination capacity. In addition, a drastic decrease of the ionic conductivity is observed beyond this peak. This trend can be well correlated to the change in the rheological behavior and the glass transition temperature with an increasing Cu(OTf)₂ concentration. At low Cu(OTf)₂ concentrations, the PDMS complex is still fluid, and its glass transition temperature is far

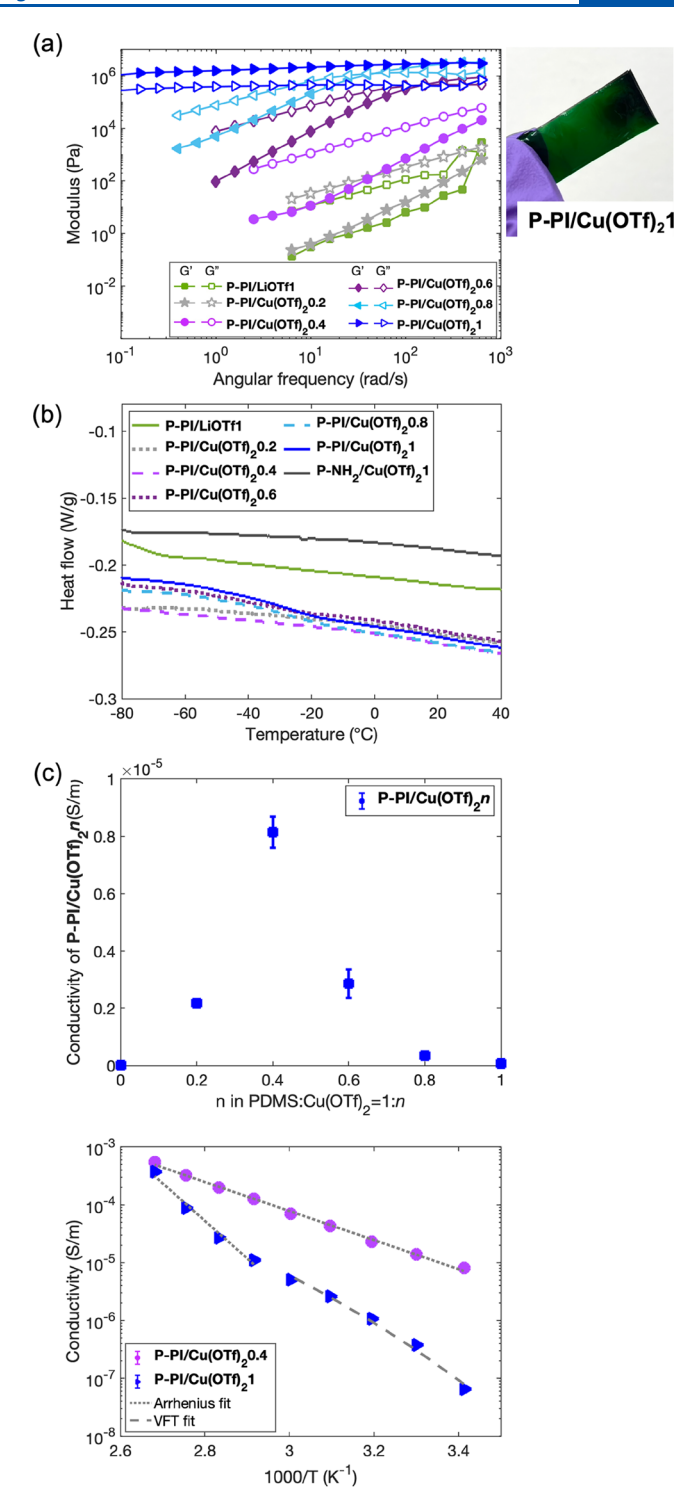


Figure 4. Cu^{2+} coordinated PDMS with different salt concentrations. (a) Frequency sweeps at a strain of 0.1% measured by rheology and a photo of a piece of $P-PI/Cu(OTf)_21$. (b) DSC curves of different PDMS complexes and of pristine PDMS mixed with $Cu(OTf)_2$ in a 1:1 molar ratio $(P-NH_2/Cu(OTf)_21)$. The latter is used as a control. (c) Variation of ionic conductivity of the polymer. (d) Ionic conductivity as a function of temperature for $P-PI/Cu(OTf)_20.4$ and $P-PI/Cu(OTf)_21$.

below room temperature ($T > T_g + 100 \,^{\circ}\text{C}$), so the fast chain segmental motion facilities the ion motion at room temperature, which is similar to the Li⁺ coordinated system. Increasing the Cu(OTf)₂ concentration from **P-PI/Cu(OTf)**₂**0.2** to **P-PI**/

 $Cu(OTf)_20.4$ improves the ion concentration and therefore increases the ionic conductivity of the material. However, the trend is interrupted by the slowing of polymer dynamics in the system at a higher $Cu(OTf)_2$ concentration. For $P-PI/Cu(OTf)_20.6$, $P-PI/Cu(OTf)_20.8$, and $P-PI/Cu(OTf)_21$, the ion motion slows due to the significantly extended chain relaxation. Another interesting observation is that the Cu^{2+} system is more ionically conductive than the Li⁺ system at the low salt concentration of PDMS:salt = 1:0.2 and 1:0.4 (Figure S26). This can be attributed to the valency of the metal cation: Cu^{2+} is balanced by two OTf^- anions, whereas Li⁺ only has one, so when adding the same number of moles of LiOTf and $Cu(OTf)_2$ salt into the PDMS, the ion concentration is higher in the Cu^{2+} system than the Li⁺ system, which promotes the high ionic conductivity.

We then examine the ionic conductivity change as a function of temperature in both P-PI/Cu(OTf)20.4 and P-PI/ Cu(OTf)₂1 (Figure 4d, Figure S27). P-PI/Cu(OTf)₂0.4 shows an Arrhenius relation similar to the Li+ system as discussed in the previous section but with a much higher apparent activation energy (48.06 kJ·mol⁻¹), which likely results from a combination of the stronger metal-ligand interaction and slower network dynamics suppressing the ion transport in the Cu²⁺ coordinated PDMS compared to the Li⁺ counterpart. However, P-PI/Cu(OTf)₂1 behaves differently, and there is an apparent trend change at around $T = T_g + 100$ °C. Given that the Arrhenius relation between ionic conductivity and temperature is valid for a temperature range of $T > T_{\rm g} + 100~{\rm ^{\circ}C}$, whereas the Vogel-Fulcher-Tammann (VFT) relation is valid for a temperature range of $T_{\rm g}$ < T < $T_{\rm g}$ + 100 °C, we believe that the factors governing the ion transport in P-PI/Cu(OTf)21 vary at different temperature ranges. At high temperatures, PDMS chain motion is reasonably fast, and thus, apparent activation energy(124.46 kJ · mol-1) is dominated by the strength of ion correlation and metal-ligand coordination. At low temperatures, ion diffusion is strongly coupled with chain

Synergistic Effect of Coordinating PDMS with Cu²⁺ and Li¹⁺. So far, the study of the Li⁺ coordinated PDMS and the Cu²⁺ coordinated PDMS has shown that the maximum ionic conductivity of each system appears at a different coordination ratio: the Li⁺ system shows the highest ionic conductivity near the saturation point, whereas the Cu²⁺ system shows the highest ionic conductivity at a much lower coordination ratio. Moreover, Cu²⁺ generates higher ionic conductivity than Li⁺ when both of them are at the same low salt concentration (the ratio of PDMS:salt = 1:0.2 and 1:0.4), because of the doubled concentration of counteranions added into the system. Given these results, a mixed Li⁺ and Cu²⁺ coordinated system with a large portion of Li⁺ and a small portion of Cu²⁺ could not only increase the ionic conductivity of the material but also enhance the mechanical properties. To verify this idea, we generate a series of ligand functionalized PDMS with both Li⁺ and Cu²⁺, and study the rheological behavior as well as the ionic conductivity of the material by varying the ratio between LiOTf and Cu(OTf)₂ (P-PI/LiOTf0.8/Cu(OTf)₂0.2 to P-PI/LiOTf0.2/Cu(OTf)₂0.8, the number after each metal indicates the mole ratio of PDMS:LiOTf:Cu(OTf)₂ = 1: m: *n*). From the rheology plots, we see that the viscoelasticity of the mixed ion coordinated PDMS is similar to that of the Cu²⁺ coordinated PDMS at the same salt concentration because the much stronger coordination of Cu²⁺ compared to Li⁺ dominates the relaxation of the dynamic network (Figure 5a). A synergistic

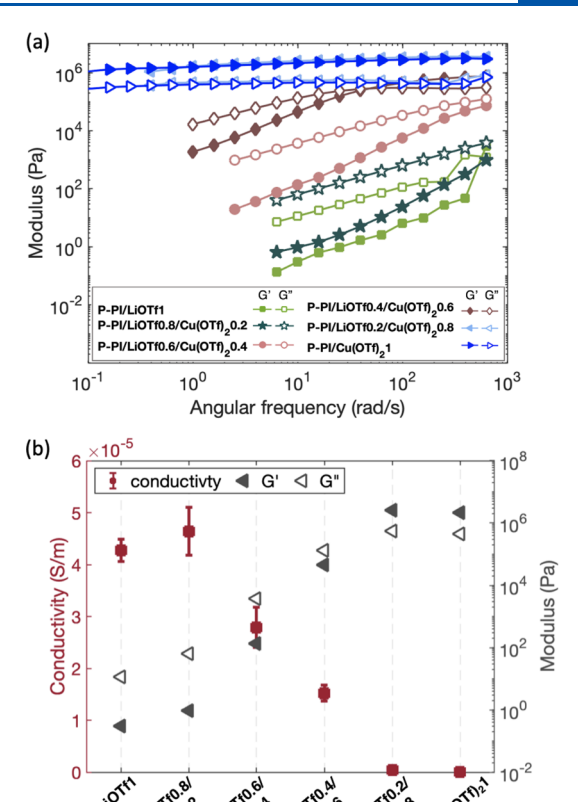


Figure 5. PDMS coordinated by mixed Li⁺ and Cu²⁺ ions. (a) Frequency sweeps at a strain of 0.1% measured by rheology. (b) Ionic conductivity of the PDMS for different ratios of Li⁺ and Cu²⁺, and the storage and loss moduli extracted from the frequency sweeps at 10 rad/

effect appears as expected when using $Cu(OTf)_2$ to replace a small amount of LiOTf in the coordinated PDMS; **P-PI/LiOTf0.8/Cu(OTf)_20.2** shows higher ionic conductivity as well as storage and loss moduli than **P-PI/LiOTf1** (Figure 5b).

CONCLUSIONS

In this work, we investigate the ion conductivity mechanism of a metal-ligand coordinated polymer by designing the model system consisting of pyridyl imine functionalized PDMS and two metal cations Li+ and Cu2+. We first confirm that the formation of metal-ligand complex promotes ion dissociation in the polymer matrix by showing increased ionic conductivity of the ligand-functionalized PDMS compared to the pristine PDMS. MD simulations prove that cation-anion dissociation is facilitated by the interaction of metal cations and ligands attached to the polymer. Based on this finding, a series of Li+ coordinated PDMS with different counteranions of the salt are synthesized to investigate the effect of cation—anion interactions on the ionic conductivity of the polymer. We find that a bulkier anion not only yields stronger Li⁺-ligand coordination but also suppresses the tendency for ion precipitation, promoting a higher ionic conductivity. In addition, MD simulations show that bulkier anions with higher delocalized charge tend to have more frequent intercluster hopping and form more negatively charged clusters. The effect of salt concentration is next studied, which is seen to enhance the ionic conductivity of the complex by increasing the ion concentration up to a point. However, for the Li⁺ cation systems, the ionic conductivity reaches the

maximum when the ligand coordination capacity is saturated and then starts to decrease at the higher salt concentrations since the additional salt preferentially forms clusters. MD simulations confirm that the chain segmental motion is also hindered by increasing salt loading, though this seemed to be a secondary influence for the Li⁺ system. The temperature-dependent ionic conductivity of the Li⁺ coordinated PDMS shows an Arrhenius relation, indicating that the strength of metal—ligand coordination and the cation—anion interaction are the rate-determining factors in the ion transport.

To investigate the effect of coordination strength on the ionic conductivity of the polymer, a series of Cu²⁺ coordinated PDMS with different salt concentrations is synthesized. From the rheological measurements, we show that as expected Cu²⁺ forms a much stronger coordination with the ligand on the PDMS than Li⁺. The Cu²⁺ coordinated PDMS transforms from a viscoelastic fluid to an elastic solid as the salt concentration increases, accompanied by a significant increase in $T_{\rm g'}$ indicating a rapid decrease in polymer dynamics. The ionic conductivity of the complex first increases with the Cu(OTf)₂ concentration but soon reaches the maximum at a low coordination ratio. Further increasing the Cu(OTf)₂ concentration leads to a sharp decrease in ionic conductivity. We attribute this to the reduction of chain mobility in the system, which limits the ion transport. In addition, at the same low salt concentration, Cu²⁺ coordinated PDMS exhibits higher ionic conductivity than Li⁺ coordinated PDMS due to the doubled concentration of mobile anions. This importance of the reduced chain mobility is in contrast to its minor role in the Li+ coordinated material. Based on these findings, an optimized metal-ligand coordinated PDMS with higher ionic conductivity and improved mechanical strength is achieved by a combination of high Li⁺ and low Cu²⁺ concentration in the system. This paper explores the structure-property relationship of the metal-ligand coordinated PDMS as a novel polymer electrolyte. At a superficial level, the governing mechanisms are similar to other polymer electrolytes (salt solvation, chain mobility, ion clustering, ion diffusion, and ion hopping); however, their relative importance and how they are controlled by the polymer structure and salt selection are quite distinct. These insights will enable more strategic future material design of low T_g ionically conductive polymers.

EXPERIMENTAL SECTION

Synthesis of Model Ligand N-Propyl(2-pyridyl)-methanimine. The model ligand N-propyl(2-pyridyl)methanimine is synthesized via a one-step condensation reaction. Under vigorous stirring at room temperature, propylamine (5.9 g, 0.1 mol) is added dropwise into a 50 mL round-bottom flask containing 2-pyridinecarboxaldehyde (10.7 g, 0.1 mol). 3A molecular sieves are added into the mixture to adsorb water. The system is reacted overnight, and the product is filtered to remove the molecular sieves, obtaining a yellow liquid (11.2 g, yield 73%). ¹H NMR: (50 MHz, CDCl₃) δ 8.62 (ddd, J = 4.9, 1.4, 1.4 Hz, 1H), 8.36 (t, J = 1.6 Hz, 1H), 7.97 (s, 1H), 7.72 (ddd, J = 7.6, 7.6, 1.7 Hz, 1H), 7.29 (ddd, J = 7.5, 4.8, 1.2 Hz, 1H), 3.63 (t, J = 6.9 Hz, 2H), 1.74 (qt, J = 7.2 Hz, 2H), 0.95 (t, J = 7.4 Hz, 3H) (Figure S2).

Synthesis of Coordination Complex LiOTf-N-Propyl(2-pyridyl)methanimine. LiOTf salt (0.39 g, 0.0025 mol) is dissolved in methanol (5 mL), and N-propyl(2-pyridyl)methanimine (0.74 g, 0.005 mol) is added into the solution. The mixture is stirred for 1 h followed by evaporating the methanol.

Synthesis of Pyridyl Imine Functionalized PDMS (P–PI). P–PI is synthesized following a previously published procedure with slight modification. ⁴² Aminopropyl terminated polydimethylsiloxane (50 g,

0.03 mol, the molecular weight is estimated from the ¹H NMR spectrum) and 2-pyridinecarboxaldehyde (7.5 g, 0.07 mol) are added into a 200 mL round-bottom flask equipped with a magnetic stir bar. Dichloromethane (50 mL) is added to the mixture as a solvent, and molecular sieves 3A (10 g) are used to adsorb water generated. The reaction proceeded at room temperature for 24 h. The mixture is then filtered to remove the molecular sieves. The obtained solution is dried under rotary evaporation to remove dichloromethane. The product is then redissolved in hexane (20 mL) and extracted by acetonitrile (50 mL) to remove excess 2-pyridinecarboxaldehyde, and the extraction is performed three times. The solution is dried under rotary evaporation to remove hexane and then left in a vacuum oven at 100 °C for 12 h to completely remove the residual solvent. The product is filtered through a 0.45 μ m PTFE filter, obtaining yellow colored PDMS oil (46 g, yield 81%). ¹H NMR: (50 MHz, CDCl₃) δ 8.67 (dt, J = 4.9, 1.4 Hz, 1H), 8.39 (t, J = 1.5 Hz, 1H), 8.01 (dt, J = 7.9, 1.1 Hz, 1H), 7.76 (td, J = 7.7, 1.8 Hz, 1H), 3.69 (td, J = 7.1, 1.4 Hz, 2H), 1.78 (ddd, J = 7.2, 6.0, 3.6 Hz, 2H), 0.68-0.52 (m, 2H), 0.09 (d, J = 2.4 Hz, 69H) (Figure S1). The molecular weight of P-PI is calculated on the basis of the integration of peaks: $69 \div 3 \times 74 + 147 \times 2 \approx 2000 \text{ g/mol.}$

Synthesis of Metal Coordinated PDMS. A vial equipped with a stir bar is used for sample preparation. In the preparation of Li coordinated PDMS, the calculated amount of Li salt is weighed and added into the pyridyl imine functionalized PDMS oil, and the mixture is stirred overnight. LiCl and LiBF₄ are not fully dissolved in the PDMS at a molar ratio of PDMS:Li salt = 1:1 even after being stirred at elevated temperature for a day. We also prepared LiCl and LiBF₄ coordinated PDMS samples with additional solvents to facilitate the dissolution. Although a transparent solution is obtained with the presence of solvents, the salt precipitates out after solvent evaporation. In the preparation of Cu²⁺ coordinated PDMS, THF is used to dissolve the calculated amount of Cu(OTf)₂ salt, and the solution is added into the PDMS oil dropwise under vigorous stirring. The mixture is stirred for 2 h to ensure thorough mixing. The solution is cast into a Teflon mold, followed by evaporating the solvent. Then the sample is transferred into a vacuum oven and dried for 24 h to ensure the complete removal of the

 ^1H Nuclear Magnetic Resonance (^1H NMR). The ^1H NMR spectrum of the ligand functionalized PDMS is acquired on a Bruker AVIII HD 500 MHz spectrometer equipped with a liquid-nitrogen cooled cryoprobe. The polymer is dissolved in CDCl $_3$ and processed by 16 scans, with 90° excitation and 30 s relaxation delay. Data are plotted in MNova (Mestrelab Research).

Liquid Chromatography Mass Spectrometry (LC-MS). The coordination complex LiOTf-N-propyl(2-pyridyl)methanimine is dissolved in methanol (5 wt/wt%) and then tee-in direct injection into the mass spectrometer is used with a flow rate of $200 \,\mu\text{L/min}$. The flow rate of the sample through the syringe pump is $10 \,\mu\text{L/min}$. A Sciex X500B is operated in electrospray ionization (ESI) positive ion Fourier transform (FT) mode, and the calibration is done with positive calibrant. ESI voltage is 5.5 kV, source temperature is 300 °C, declustering potential is 50 V, and accumulation time is 0.15 s. An MS full scan from m/z 100 to m/z 1000 in profile mode was acquired from 0 to 5 min. Time-of-flight mass spectrometry (TOF MS/MS) is also acquired at the mass range of m/z 100 to m/z 1000 from 0 to 5 min.

Fourier-Transform Infrared (FTIR) Spectroscopy. The IR spectra of the materials are collected by a Bruker Vertex V80 V Vacuum FTIR system under the attenuated total reflection (ATR) configuration. The spectral ranges of 4000 cm⁻¹ to 600 cm⁻¹ are collected.

Electrochemical Impedance Spectroscopy (EIS). The metalligand coordinated PDMS samples are sandwiched between two pieces of gold coated ${\rm SiO_2}$ substrates with $100~\mu{\rm m}$ Teflon sheet spacers placed on both sides. The gold electrode had an area of 1 cm². The samples are characterized with the Reference 3000AE potentiostat from Gamry Instruments. A sinusoidal voltage with an amplitude of 50 mV is applied in the frequency range of 1 Hz to 1 MHz. The bulk impedance is read from the data point on the Nyquist plot at the right of the first circle and closest to the real axis. This data point is read using Gamry's Echem Analyst software. We then calculate the conductivity using the equation

 $\sigma = ((l)/(RA))$ where l is the separation of our electrodes (100 μ m), A is the area of our electrodes (1 cm²), and R is the extracted bulk impedance.

Dielectric Spectroscopy. Dielectric constants for P-PI and P-NH₂ were measured using a Keysight 16451B dielectric test fixture and a 3000AE Gamry potentiostat. The test fixture was calibrated according to the Keysight reference manual, using air as a reference dielectric. A sinusoidal voltage with an RMS amplitude of 1 V was applied over a range of 1 Hz to 1 MHz. For P-PI, a capacitor was fit to the impedance data in the Gamry Framework software, and the dielectric was calculated from the geometry of the test fixture and the calibration values according to the equation $\epsilon = (C - C_w)t/A\epsilon_0$, where C is the fit capacitance, $C_{\rm w}$ is the calibrated stray wire capacitance, t is the parallel plate separation, A is the area of each plate, and ϵ_0 is the free space permittivity. For our setup, $C_{\rm w} = 150$ pf. Measurements were taken with three parallel plate separations (0.1 mm, 0.15 mm, and 0.2 mm) and averaged to produce a final dielectric constant. For P-NH2, because there was evidence of some conductivity, a parallel resistor-capacitor circuit was fit instead. The capacitance and equation were again used to calculate the dielectric constant.

VLFEIS Transference Number. Symmetric lithium cells were made for transference number measurements. 100 μL portion of the sample solution was added to each cell, with Whatman glass fiber grade GF/B used as the separator. The glass fiber separators were first dried under 100 °C for 24 h before use to remove the moisture. Lithium foil (purchased from Alfa Aesar, 99.9% metals basis) was cut into disks with a diameter of 0.25 in. and used as the metal electrodes directly. The entire cell assembly was done in an argon-filled glovebox. Each cell first rested for 24 h, and then was conditioned with 200 nA for 60 s and -200 nA for 60 s. EIS with an RMS amplitude of 1 mV was performed from 1 mHz to 1 MHz. An equivalent circuit consisting of 4 CPE–resistor pairs was fit to the data, and the transference number was calculated as $R_{\rm diffusion}/(R_{\rm diffusion}+R_{\rm bulk})$. The details of this fit are presented in section 4.5 of the SI.

Pulsed-Field-Gradient (PFG) Spin-Echo (SE) NMR. Diffusion experiments are performed on a Varian INOVA 600 spectrometer operating at 599.50 and 564.01 MHz for ¹H and ¹⁹F observation, respectively, equipped with a Nalorac broadband H/F probe with a double tuned outer coil. All experiments are performed at 100 °C to obtain good signals, and all the samples of PDMS complexes are directly injected into the NMR tubes without adding solvent. ¹H diffusion experiments are performed with the convection-compensated, bipolargradient double stimulated-echo (Dbppste cc) pulse sequence, modified to include a 5 ms longitudinal eddy current delay. Sixteen gradient values are collected with 2 steady-state scans and 4 scans for each increment. The acquisition time is 1.3 s, and the relaxation delay is 4 s. The diffusion gradient pulse length (δ) is 4 ms, and the diffusion delay (Δ) is 200 to 800 ms to ensure that at least three half-lives are acquired. 19F diffusion experiments are performed with the convectioncompensated double stimulated-echo (DgcsteSL cc) pulse sequence. Sixteen gradient values are collected with 2 steady-state scans and 4 scans for each increment. The acquisition time is 1.0 s, and the relaxation delay is 2 s. The diffusion gradient pulse length (δ) is between 3 and 4 ms, and the diffusion delay (Δ) is 750 to 1500 ms to ensure that at least three half-lives are acquired. Data is analyzed in MNova (Mestrelab Research). The diffusion coefficient of the PDMS backbone in each sample is calculated on the basis of a single exponential fit of the change of peak area integral in the ¹H diffusion experiment, and an average of the diffusion coefficients calculated from different peaks representing different moieties is used as the final value. The diffusion coefficient of counteranions in each sample is calculated on the basis of a single exponential fit of the change of peak area integral in the ¹⁹F diffusion experiment.

Rheology. The rheology of the materials is measured by a TA Instruments DHR-3 rheometer with a 40 mm-diameter parallel plate. ~ 1.26 mL sample is added to the stage with 2 mm thickness. Before each measurement, the sample is first equilibrated at 25 °C for 10 min. A strain sweep is performed at a frequency of 1 Hz. A frequency sweep is performed with a strain amplitude of 0.1%.

Differential Scanning Calorimeter (DSC). The glass transition temperature of the polymer is tested by a TA Instruments DSC Auto 2500. The samples are loaded in Tzero aluminum pans and measured with a heating rate of 10 °C/min and a cooling rate of 5 °C/min from -90 to 120 °C for one heating–cooling—heating cycle. Data from the second heating process is used. The glass transition temperature of each sample $(T_{\rm g})$ is determined from the midpoint of the transition on the heat flow curve.

Molecular Dynamics Simulation Setup and Equilibration. The fully atomistic MD simulations are performed with LAMMPS. Each simulated system consists of 20 PDMS chains, each with 21 monomers long; 20 salt pairs are doped into the system for the PDMS:salt = 1:1 case. For each salt species, we considered 9 randomized trajectories from 3 different initial configurations and 3 different initial velocity seeds.⁷⁵

Force field parameters and initial configurations for the PDMS and ions are generated with the Enhanced Monte Carlo software 76 using the PCFF framework.⁵⁰ The point charge assigned to the ion pairs is rescaled by 0.7. The charge downscale procedure is commonly used for classical force fields, where a static point-charge model can lead to an exaggeration of ionic interaction strength. The velocity-Verlet integrator with a time step of 0.5 fs is used for motion evolution; this value is selected as the largest one, ensuring reasonable drift of atoms within a single time step. The relaxation process consists of the steepest descent and conjugate gradient energy minimization, followed by equilibration in the canonical (nVT) and isothermal-isobaric (nPT) statistical ensembles at the target temperature and pressure of 303 K and 1 bar, for a total duration of 5 ns. The Nose-Hoover thermostats and barostats are used with damping parameters set to 50 and 500 fs, respectively. The production run is conducted in the nVT ensemble at 303 K for 50 ns, except for the diffusion coefficient comparison with experimental results, which was conducted at 373 K. For nonbonded interactions, long-range electrostatic interactions are calculated by using the particle-particle particle-mesh solver with a 1.2 nm cutoff distance, while Lennard-Jones interactions are truncated at 1.2 nm with the long-range van der Waals tail corrections included for energy and pressure modification.

Molecular Dynamics Cluster and Ionic Conductivity Analysis. The self-diffusion coefficient is calculated using the Einstein relation:

$$D_{\text{ion}} = \lim_{t \to \infty} \frac{\left\langle \frac{1}{N} \sum_{i=1}^{N} \left| \mathbf{x}_i(t_0 + t) - \mathbf{x}_i(t_0) \right|^2 \right\rangle_{c, t_0}}{6t}$$
(1)

where \mathbf{x}_i (t) is the instantaneous position of i^{th} particle at time t and N is the number of particles. The numerator is mean-squared displacement (MSD) of a molecule center of mass during time t and $\langle ... \rangle$ denotes an ensemble average. Note that we performed both configuration averaging and time-origin averaging using a sliding-window strategy. The relation only holds for the Fickian regime of the MSD curve; therefore, it is necessary to reach the diffusive linear regime to extract an accurate diffusion coefficient. The strategy of the matter of th

With the diffusion coefficients for mobile species obtained from MSD, we first calculate the ionic conductivity with the Nernst–Einstein equation, which states that the total conductivity is proportional to individual diffusion coefficient and ionic concentration:

$$\sigma_{\rm NE} = \frac{e^2}{V k_{\rm B} T} (N_{+} z_{+}^2 D_{+} + N_{-} z_{-}^2 D_{-})$$
 (2)

where $k_{\rm B}$ is the Boltzmann constant, e is the elementary charge, V is the volume of simulation box, T is the temperature, z_{\pm} and N_{\pm} is the charge and number of cations and anions. However, the NE equation assumes ions do not interact with themselves and is therefore only exact in the infinite dilution limit. For electrolytes with high salt concentrations, ionic transport shifts from single free charge carriers to clusters of salt nucleating, which has the primary function of scaling down the conductivity by forming neutral clusters. To account for the effect of clustering, Grossman et al. reformulated the Nernst–Einstein equation with the assumption that clusters do not interact with each other: 34

$$\sigma_{\text{cNE}} = \frac{e^2}{V k_{\text{B}} T} \sum_{i=0}^{N_{+}} \sum_{j=0}^{N_{-}} z_{ij}^2 \alpha_{ij} D_{ij}$$
(3)

where the fundamental charge carriers are no longer single free ions but ionic clusters of different charge numbers $z_{ij} = iz_+ + jz_-$. α_{ij} is the matrix element that defines the population of the cluster consisting of i cations and j anions, which is averaged over ensembles and a long simulation time. D_{ij} is the diffusion coefficient for each type of cluster written in the matrix form. Cation(s) and anion(s) are defined to belong to the same cluster if the cation is within the cutoff distance of one or more of the anions. It is worth noting that neutral clusters with $z_{ij} = 0$ do not contribute to the total conductivity, although it also diffuses. This is the first time that the cluster Nernst–Einstein (cNE) is applied to a polymer-in-salt system other than PEO or PEO-based variants. 62

Molecular Dynamics Ion Hopping Analysis. The ion hopping analysis is characterized by tracking the coordination environment change of a single ion. Time-dependent trajectory of cation coordination is traced on the basis of a distance criterion (i.e., an atom contributes to the coordination of a cation when its distance to the cation is less than the coordination cutoff). Specifically, the coordination from the most electronegative nitrogen atoms of the polymer chains and the oxygen atoms of the anions is tracked over the simulation time. The consecutive indices correspond to consecutive coordination from the same chain or anion, while the switch between two different consecutive lines indicates a cation jump among chains.

ASSOCIATED CONTENT

Supporting Information

The Supporting Information is available free of charge at https://pubs.acs.org/doi/10.1021/acs.macromol.2c02519.

Experimental methods and characterization data (PDF)

AUTHOR INFORMATION

Corresponding Author

Meredith N. Silberstein — Sibley School of Mechanical and Aerospace Engineering, Cornell University, Ithaca, New York 14853, United States; ⊚ orcid.org/0000-0002-6853-9796; Email: meredith.silberstein@cornell.edu

Authors

Xinyue Zhang — Department of Materials Science and Engineering, Cornell University, Ithaca, New York 14850, United States

Jinyue Dai — Sibley School of Mechanical and Aerospace Engineering, Cornell University, Ithaca, New York 14853, United States; oorcid.org/0000-0002-4878-8373

Max Tepermeister — Sibley School of Mechanical and Aerospace Engineering, Cornell University, Ithaca, New York 14853, United States

Yue Deng — Department of Materials Science and Engineering, Cornell University, Ithaca, New York 14850, United States Jingjie Yeo — Sibley School of Mechanical and Aerospace Engineering, Cornell University, Ithaca, New York 14853, United States; orcid.org/0000-0002-6462-7422

Complete contact information is available at: https://pubs.acs.org/10.1021/acs.macromol.2c02519

Author Contributions

¶(X.Z., J.D.) These authors contributed equally to this work.

The authors declare no competing financial interest.

ACKNOWLEDGMENTS

The authors thank the support from Defense Advanced Research Project Agency Young Faculty Award (DARPA YFA; HR00112010004). This research made use of the Cornell Center for Materials Research Shared Facilities which are supported through the NSF MRSEC program (DMR-1719875). This work used Stampede2 supercomputing through allocation TG-MSS140006 from the Extreme Science and Engineering Discovery Environment (XSEDE), which was supported by National Science Foundation grant number #1548562. This work is performed in part at the Cornell NanoScale Facility, a member of the National Nanotechnology Coordinated Infrastructure (NNCI), which is supported by the National Science Foundation (Grant NNCI-2025233). The authors acknowledge Ivan Keresztes for helping perform PFG SE NMR.

REFERENCES

- (1) Zhu, J.; Zhang, Z.; Zhao, S.; Westover, A. S.; Belharouak, I.; Cao, P.-F. Single-ion conducting polymer electrolytes for solid–state lithium-metal batteries: design, performance, and challenges. *Adv. Energy Mater.* **2021**, *11*, 2003836.
- (2) Wang, J.; Gao, D.; Lee, P. S. Recent progress in artificial muscles for interactive soft robotics. *Adv. Mater.* **2021**, *33*, 2003088.
- (3) Ma, S.; Zhang, Y.; Liang, Y.; Ren, L.; Tian, W.; Ren, L. High-performance ionic-polymer-metal composite: toward large-deformation fast-response artificial muscles. *Adv. Funct. Mater.* **2020**, *30*, 1908508.
- (4) Xiao, K.; Wan, C.; Jiang, L.; Chen, X.; Antonietti, M. Bioinspired ionic sensory systems: the successor of electronics. *Adv. Mater.* **2020**, 32, 2000218.
- (5) Tepermeister, M.; Bosnjak, N.; Dai, J.; Zhang, X.; Kielar, S. M.; Wang, Z.; Tian, Z.; Suntivich, J.; Silberstein, M. N. Soft Ionics: Governing Physics and State of Technologies. *Frontiers in Physics* **2022**, *11*, 890845.
- (6) Armand, M. Polymers with ionic conductivity. *Adv. Mater.* **1990**, *2*, 278–286.
- (7) Jiang, Y.; Yan, X.; Ma, Z.; Mei, P.; Xiao, W.; You, Q.; Zhang, Y. Development of the PEO based solid polymer electrolytes for all-solid state lithium ion batteries. *Polymers* **2018**, *10*, 1237.
- (8) Ohno, H.; Yoshizawa, M.; Ogihara, W. Development of new class of ion conductive polymers based on ionic liquids. *Electrochim. Acta* **2004**, *50*, 255–261.
- (9) Qian, W.; Texter, J.; Yan, F. Frontiers in poly (ionic liquid) s: syntheses and applications. *Chem. Soc. Rev.* **2017**, *46*, 1124–1159.
- (10) Bhandari, B.; Lee, G.-Y.; Ahn, S.-H. A review on IPMC material as actuators and sensors: fabrications, characteristics and applications. *International journal of precision engineering and manufacturing* **2012**, *13*, 141–163.
- (11) Schauser, N. S.; Seshadri, R.; Segalman, R. A. Multivalent ion conduction in solid polymer systems. *Molecular Systems Design & Engineering* **2019**, *4*, 263–279.
- (12) Shin, J.-H.; Henderson, W. A.; Passerini, S. Ionic liquids to the rescue? Overcoming the ionic conductivity limitations of polymer electrolytes. *Electrochem. Commun.* **2003**, *5*, 1016–1020.
- (13) Imbrogno, J.; Maruyama, K.; Rivers, F.; Baltzegar, J. R.; Zhang, Z.; Meyer, P. W.; Ganesan, V.; Aoshima, S.; Lynd, N. A. Relationship between Ionic Conductivity, Glass Transition Temperature, and Dielectric Constant in Poly (vinyl ether) Lithium Electrolytes. ACS Macro Lett. 2021, 10, 1002–1007.
- (14) Shen, K.-H.; Hall, L. M. Effects of ion size and dielectric constant on ion transport and transference number in polymer electrolytes. *Macromolecules* **2020**, *53*, 10086–10096.
- (15) Wojtecki, R. J.; Meador, M. A.; Rowan, S. J. Using the dynamic bond to access macroscopically responsive structurally dynamic polymers. *Nature materials* **2011**, *10*, 14–27.

- (16) Grindy, S. C.; Learsch, R.; Mozhdehi, D.; Cheng, J.; Barrett, D. G.; Guan, Z.; Messersmith, P. B.; Holten-Andersen, N. Control of hierarchical polymer mechanics with bioinspired metal-coordination dynamics. *Nature materials* **2015**, *14*, 1210–1216.
- (17) Li, C.-H.; Zuo, J.-L. Self-healing polymers based on coordination bonds. *Adv. Mater.* **2020**, *32*, 1903762.
- (18) Khare, E.; Holten-Andersen, N.; Buehler, M. J. Transition-metal coordinate bonds for bioinspired macromolecules with tunable mechanical properties. *Nature Reviews Materials* **2021**, *6*, 421–436.
- (19) Zhang, X.; Vidavsky, Y.; Aharonovich, S.; Yang, S. J.; Buche, M. R.; Diesendruck, C. E.; Silberstein, M. N. Bridging experiments and theory: isolating the effects of metal-ligand interactions on viscoelasticity of reversible polymer networks. *Soft Matter* **2020**, *16*, 8591–8601.
- (20) Zhang, X.; Crisci, R.; Finlay, J. A.; Cai, H.; Clare, A. S.; Chen, Z.; Silberstein, M. N. Enabling Tunable Water-Responsive Surface Adaptation of PDMS via Metal—Ligand Coordinated Dynamic Networks. *Advanced Materials Interfaces* **2022**, *9*, 2200430.
- (21) Wang, H.-N.; Meng, X.; Dong, L.-Z.; Chen, Y.; Li, S.-L.; Lan, Y.-Q. Coordination polymer-based conductive materials: ionic conductivity vs. electronic conductivity. *Journal of Materials Chemistry A* **2019**, *7*, 24059–24091.
- (22) Sanoja, G. E.; Schauser, N. S.; Bartels, J. M.; Evans, C. M.; Helgeson, M. E.; Seshadri, R.; Segalman, R. A. Ion transport in dynamic polymer networks based on metal-ligand coordination: effect of cross-linker concentration. *Macromolecules* **2018**, *51*, 2017–2026.
- (23) Schauser, N. S.; Sanoja, G. E.; Bartels, J. M.; Jain, S. K.; Hu, J. G.; Han, S.; Walker, L. M.; Helgeson, M. E.; Seshadri, R.; Segalman, R. A. Decoupling bulk mechanics and mono-and multivalent ion transport in polymers based on metal-ligand coordination. *Chem. Mater.* **2018**, *30*, 5759–5769.
- (24) Schauser, N. S.; Grzetic, D. J.; Tabassum, T.; Kliegle, G. A.; Le, M. L.; Susca, E. M.; Antoine, S.; Keller, T. J.; Delaney, K. T.; Han, S.; et al. The role of backbone polarity on aggregation and conduction of ions in polymer electrolytes. *J. Am. Chem. Soc.* **2020**, *142*, 7055–7065.
- (25) Anderson, E. B.; Long, T. E. Imidazole-and imidazolium-containing polymers for biology and material science applications. *Polymer* **2010**, *51*, 2447–2454.
- (26) Nikolaev, A.; Richardson, P. M.; Xie, S.; Canzian Llanes, L.; Jones, S. D.; Nordness, O.; Wang, H.; Bazan, G. C.; Segalman, R. A.; Clément, R. J.; et al. Role of Electron-Deficient Imidazoles in Ion Transport and Conductivity in Solid-State Polymer Electrolytes. *Macromolecules* **2022**, *55*, 971–977.
- (27) Zhou, W.; Wang, Z.; Pu, Y.; Li, Y.; Xin, S.; Li, X.; Chen, J.; Goodenough, J. B. Double-layer polymer electrolyte for high-voltage all-solid-state rechargeable batteries. *Adv. Mater.* **2019**, *31*, 1805574.
- (28) Lu, G.; Qiu, H.; Du, X.; Sonigara, K. K.; Wang, J.; Zhang, Y.; Chen, Z.; Chen, L.; Ren, Y.; Zhao, Z.; et al. Heteroleptic Coordination Polymer Electrolytes Initiated by Lewis-Acidic Eutectics for Solid Zinc–Metal Batteries. *Chem. Mater.* **2022**, *34*, 8975–8986.
- (29) Dünweg, B.; Kremer, K. Molecular dynamics simulation of a polymer chain in solution. *J. Chem. Phys.* **1993**, *99*, 6983–6997.
- (30) Shen, K.-H.; Fan, M.; Hall, L. M. Molecular dynamics simulations of ion-containing polymers using generic coarse-grained models. *Macromolecules* **2021**, *54*, 2031–2052.
- (31) Boden, N.; Leng, S.; Ward, I. Ionic conductivity and diffusivity in polyethylene oxode/electrolyte solutions as models for polymer electrolytes. *Solid State Ionics* **1991**, *45*, 261–270.
- (32) Molinari, N.; Mailoa, J. P.; Kozinsky, B. Effect of salt concentration on ion clustering and transport in polymer solid electrolytes: a molecular dynamics study of peo-litfsi. *Chem. Mater.* **2018**, *30*, 6298–6306.
- (33) Wheeler, D. R.; Newman, J. Molecular dynamics simulations of multicomponent diffusion. 1. Equilibrium method. *J. Phys. Chem. B* **2004**. *108*. 18353–18361.
- (34) France-Lanord, A.; Grossman, J. C. Correlations from ion pairing and the Nernst-Einstein equation. *Physical review letters* **2019**, 122, 136001.

- (35) Gupta, N. S.; Lee, K.-S.; Labouriau, A. Tuning Thermal and Mechanical Properties of Polydimethylsiloxane with Carbon Fibers. *Polymers* **2021**, *13*, 1141.
- (36) Bresser, D.; Lyonnard, S.; Iojoiu, C.; Picard, L.; Passerini, S. Decoupling segmental relaxation and ionic conductivity for lithium-ion polymer electrolytes. *Molecular Systems Design & Engineering* **2019**, 4, 779–792.
- (37) Companik, J.; Bidstrup, S. The viscosity and ion conductivity of polydimethylsiloxane systems: 2. Ion concentration effects. *Polymer* **1994**, 35, 4834–4841.
- (38) Othman, M. B. H.; Ramli, M. R.; Tyng, L. Y.; Ahmad, Z.; Akil, H. M. Dielectric constant and refractive index of poly (siloxane–imide) block copolymer. *Materials & Design* **2011**, 32, 3173–3182.
- (39) Fong, K. D.; Self, J.; McCloskey, B. D.; Persson, K. A. Ion correlations and their impact on transport in polymer-based electrolytes. *Macromolecules* **2021**, *54*, 2575–2591.
- (40) Qi, D.; Zhang, K.; Tian, G.; Jiang, B.; Huang, Y. Stretchable electronics based on PDMS substrates. *Adv. Mater.* **2021**, *33*, 2003155.
- (41) Pignanelli, J.; Qian, Z.; Gu, X.; Ahamed, M. J.; Rondeau-Gagné, S. Modulating the thermomechanical properties and self-healing efficiency of siloxane-based soft polymers through metal-ligand coordination. *New J. Chem.* **2020**, *44*, 8977–8985.
- (42) Pignanelli, J.; Billet, B.; Straeten, M.; Prado, M.; Schlingman, K.; Ahamed, M. J.; Rondeau-Gagné, S. Imine and metal—ligand dynamic bonds in soft polymers for autonomous self-healing capacitive-based pressure sensors. *Soft Matter* **2019**, *15*, 7654—7662.
- (43) Yuan, K.; Bian, H.; Shen, Y.; Jiang, B.; Li, J.; Zhang, Y.; Chen, H.; Zheng, J. Coordination number of Li+ in nonaqueous electrolyte solutions determined by molecular rotational measurements. *J. Phys. Chem. B* **2014**, *118*, 3689–3695.
- (44) Ueno, N.; Wakabayashi, T.; Morisawa, Y. Determining the coordination number of Li+ and glyme or poly (ethylene glycol) in solution using attenuated total reflectance-far ultraviolet spectroscopy. *Anal. Sci.* **2019**, *36*, 91–93.
- (45) Jun, M.-S.; Choi, Y.-W.; Kim, J.-D. Solvent casting effects of sulfonated poly (ether ether ketone) for Polymer electrolyte membrane fuel cell. *J. Membr. Sci.* **2012**, *396*, 32–37.
- (46) Bodas, D.; Khan-Malek, C. Formation of more stable hydrophilic surfaces of PDMS by plasma and chemical treatments. *Microelectronic engineering* **2006**, 83, 1277—1279.
- (47) Smith, G.; Chen, R.; Mapolie, S. The synthesis and catalytic activity of a first-generation poly (propylene imine) pyridylimine palladium metallodendrimer. *J. Organomet. Chem.* **2003**, *673*, 111–115.
- (48) Johnston, D. H.; Shriver, D. F. Vibrational study of the trifluoromethanesulfonate anion: unambiguous assignment of the asymmetric stretching modes. *Inorg. Chem.* **1993**, 32, 1045–1047.
- (49) Plimpton, S. Fast parallel algorithms for short-range molecular dynamics. *J. Comput. Phys.* **1995**, *117*, 1–19.
- (50) Sun, H. Force field for computation of conformational energies, structures, and vibrational frequencies of aromatic polyesters. *J. Comput. Chem.* **1994**, *15*, 752–768.
- (51) Olsher, U.; Izatt, R. M.; Bradshaw, J. S.; Dalley, N. K. Coordination chemistry of lithium ion: a crystal and molecular structure review. *Chem. Rev.* **1991**, *91*, 137–164.
- (52) Humphrey, W.; Dalke, A.; Schulten, K. VMD: visual molecular dynamics. *J. Mol. Graphics* **1996**, *14*, 33–38.
- (53) Eisenberg, A. Clustering of ions in organic polymers. A theoretical approach. *Macromolecules* **1970**, *3*, 147–154.
- (54) Borodin, O.; Smith, G. D. Mechanism of ion transport in amorphous poly (ethylene oxide)/LiTFSI from molecular dynamics simulations. *Macromolecules* **2006**, *39*, 1620–1629.
- (55) Rao, Y.-L.; Feig, V.; Gu, X.; Nathan Wang, G.-J.; Bao, Z. The effects of counter anions on the dynamic mechanical response in polymer networks crosslinked by metal-ligand coordination. *J. Polym. Sci., Part A: Polym. Chem.* **2017**, *55*, 3110–3116.
- (56) Chu, T.; Belding, L.; van der Est, A.; Dudding, T.; Korobkov, I.; Nikonov, G. I. A Coordination Compound of Ge0 Stabilized by a Diiminopyridine Ligand. *Angew. Chem., Int. Ed.* **2014**, *53*, 2711–2715.

- (57) Kim, K.; Kuhn, L.; Alabugin, I. V.; Hallinan, D. T., Jr Lithium salt dissociation in diblock copolymer electrolyte using fourier transform infrared spectroscopy. *Frontiers in Energy Research* **2020**, *8*, 569442.
- (58) Cheng, Y.; Yang, J.; Hung, J.-H.; Patra, T. K.; Simmons, D. S. Design rules for highly conductive polymeric ionic liquids from molecular dynamics simulations. *Macromolecules* **2018**, *51*, 6630–6644.
- (59) Bocharova, V.; Sokolov, A. P. Perspectives for polymer electrolytes: a view from fundamentals of ionic conductivity. *Macromolecules* **2020**, *53*, 4141–4157.
- (60) Fujie, K.; Ikeda, R.; Otsubo, K.; Yamada, T.; Kitagawa, H. Lithium ion diffusion in a metal—organic framework mediated by an ionic liquid. *Chem. Mater.* **2015**, *27*, 7355–7361.
- (61) Wohde, F.; Balabajew, M.; Roling, B. Li+ Transference Numbers in Liquid Electrolytes Obtained by Very-Low-Frequency Impedance Spectroscopy at Variable Electrode Distances. *Journal of The Electrochemical Society* **2016**, *163*, A714.
- (62) France-Lanord, A.; Wang, Y.; Xie, T.; Johnson, J. A.; Shao-Horn, Y.; Grossman, J. C. Effect of chemical variations in the structure of poly (ethylene oxide)-based polymers on lithium transport in concentrated electrolytes. *Chem. Mater.* **2020**, 32, 121–126.
- (63) Mindemark, J.; Lacey, M. J.; Bowden, T.; Brandell, D. Beyond PEO—Alternative host materials for Li+-conducting solid polymer electrolytes. *Prog. Polym. Sci.* **2018**, *81*, 114–143.
- (64) Gouverneur, M.; Schmidt, F.; Schönhoff, M. Negative effective Li transference numbers in Li salt/ionic liquid mixtures: does Li drift in the "Wrong" direction? *Phys. Chem. Chem. Phys.* **2018**, 20, 7470–7478.
- (65) Forsyth, M.; Payne, V.; Ratner, M.; De Leeuw, S.; Shriver, D. Molecular dynamics simulations of highly concentrated salt solutions: Structural and transport effects in polymer electrolytes. *Solid State Ionics* **1992**, 53, 1011–1026.
- (66) Xie, L.; Farrington, G. Molecular mechanics and dynamics simulation of poly (ethylene oxide) electrolytes. *Solid State Ionics* **1992**, 53, 1054–1058.
- (67) Hu, Z.; Kerton, F. M. Room temperature aerobic oxidation of alcohols using CuBr2 with TEMPO and a tetradentate polymer based pyridyl-imine ligand. *Applied Catalysis A: General* **2012**, *413*, 332–339.
- (68) Zuidema, J. M.; Rivet, C. J.; Gilbert, R. J.; Morrison, F. A. A protocol for rheological characterization of hydrogels for tissue engineering strategies. *Journal of Biomedical Materials Research Part B: Applied Biomaterials* **2014**, *102*, 1063–1073.
- (69) Rubinstein, M.; Colby, R. H. et al. *Polymer Physics*; Oxford University Press: New York, 2003; Vol. 23.
- (70) Ratner, M. A.; Shriver, D. F. Ion transport in solvent-free polymers. *Chem. Rev.* **1988**, *88*, 109–124.
- (71) Schlenoff, J. B.; Akkaoui, K. Dissecting dynamics near the glass transition using polyelectrolyte complexes. *Macromolecules* **2021**, *54*, 3413–3422.
- (72) Chen, H.; Choi, J.-H.; Salas-de la Cruz, D.; Winey, K. I.; Elabd, Y. A. Polymerized ionic liquids: the effect of random copolymer composition on ion conduction. *Macromolecules* **2009**, *42*, 4809–4816.
- (73) Klein, R. J.; Zhang, S.; Dou, S.; Jones, B. H.; Colby, R. H.; Runt, J. Modeling electrode polarization in dielectric spectroscopy: Ion mobility and mobile ion concentration of single-ion polymer electrolytes. *J. Chem. Phys.* **2006**, *124*, 144903.
- (74) Stacy, E. W.; Gainaru, C. P.; Gobet, M.; Wojnarowska, Z.; Bocharova, V.; Greenbaum, S. G.; Sokolov, A. P. Fundamental limitations of ionic conductivity in polymerized ionic liquids. *Macromolecules* **2018**, *51*, 8637–8645.
- (75) Wang, J.; Hou, T. Application of molecular dynamics simulations in molecular property prediction II: Diffusion coefficient. *Journal of computational chemistry* **2011**, *32*, 3505–3519.
- (76) in't Veld, P. J.; Rutledge, G. C. Temperature-dependent elasticity of a semicrystalline interphase composed of freely rotating chains. *Macromolecules* **2003**, *36*, 7358–7365.
- (77) Leontyev, I.; Stuchebrukhov, A. Accounting for electronic polarization in non-polarizable force fields. *Phys. Chem. Chem. Phys.* **2011**, *13*, 2613–2626.
- (78) Fick, A. Ueber diffusion. Annalen der Physik 1855, 170, 59-86.

☐ Recommended by ACS

Toughening Ionic Polymer Using Bulky Alkylammonium Counterions and Comb Architecture

Daisuke Aoki, Koji Arimitsu, et al.

MARCH 24, 2023

ACS MACRO LETTERS

READ 🗹

Self-Healing, Recyclable, and Degradable Castor Oil-Based Elastomers for Sustainable Soft Robotics

Aleix Costa Cornellà, Joost Brancart, et al.

FEBRUARY 10, 2023

ACS SUSTAINABLE CHEMISTRY & ENGINEERING

READ 🗹

Fragile Glass Formation and Non-Arrhenius Upturns in Ethylene Vitrimers Revealed by Dielectric Spectroscopy

Bhaskar Soman, Christopher M. Evans, et al.

DECEMBER 16, 2022

MACROMOLECULES

READ 🗹

Degradable and Nanosegregated Elastomers with Multiblock Sequences of Biobased Aromatic Mesogens and Biofunctional Aliphatic Oligocarbonates

Yuya Watanabe, Takashi Kato, et al.

NOVEMBER 15, 2022

MACROMOLECULES

READ 🗹

Get More Suggestions >